Jeffrey L. Braun
Department of Mechanical and Aerospace Engineering, University of Virginia, Charlottesville, VA 22904

Chester J. Szwejkowski
Department of Mechanical and Aerospace Engineering, University of Virginia, Charlottesville, VA 22904

Ashutosh Giri
Department of Mechanical and Aerospace Engineering, University of Virginia, Charlottesville, VA 22904

Patrick E. Hopkins[1]
Department of Mechanical and Aerospace Engineering, University of Virginia, Charlottesville, VA 22904; Department of Materials Science and Engineering, University of Virginia, Charlottesville, VA 22904; Department of Physics, University of Virginia, Charlottesville, VA 22904
e-mail: phopkins@virginia.edu

On the Steady-State Temperature Rise During Laser Heating of Multilayer Thin Films in Optical Pump–Probe Techniques

In this study, we calculate the steady-state temperature rise that results from laser heating of multilayer thin films using the heat diffusion equation. For time- and frequency-domain thermoreflectance (TDTR and FDTR) that rely on modulated laser sources, we decouple the modulated and steady-state temperature profiles to understand the conditions needed to achieve a single temperature approximation throughout the experimental volume, allowing for the estimation of spatially invariant thermal parameters within this volume. We consider low thermal conductivity materials, including amorphous silicon dioxide (a-SiO_2), polymers, and disordered C_{60}, to demonstrate that often-used analytical expressions fail to capture this temperature rise under realistic experimental conditions, such as when a thin-film metal transducer is used or when pump and probe spot sizes are significantly different. To validate these findings and demonstrate a practical approach to simultaneously calculate the steady-state temperature and extract thermal parameters in TDTR, we present an iterative algorithm for obtaining the steady-state temperature rise and measure the thermal conductivity and thermal boundary conductance of a-SiO_2 with a 65-nm gold thin film transducer. Furthermore, we discuss methods of heat dissipation to include the use of conductive substrates as well as the use of bidirectional heat flow geometries. Finally, we quantify the influence of the optical penetration depth (OPD) on the steady-state temperature rise to reveal that only when the OPD approaches the characteristic length of the temperature decay does it alter the temperature profile relative to the surface heating condition. [DOI: 10.1115/1.4038713]

1 Introduction

In optical pump–probe techniques such as time- and frequency-domain thermoreflectance (TDTR and FDTR, respectively), the measurement of bulk, low-thermal conductivity materials is challenging due to the steady-state temperature rise associated with the average power absorbed during laser heating. In such experiments, an estimate of this temperature rise is crucial since thermal properties can vary significantly with temperature. Because fitting procedures can be highly sensitive to these temperature-dependent input parameters, neglecting the temperature rise can result in large errors of fitted parameters. This is particularly important at low temperatures where heat capacities and thermal conductivities are highly temperature dependent [1]. Moreover, appropriate modeling of the temperature rise is needed in many cases for determining critical temperatures like phase transition temperatures and damage thresholds. For example, many polymers have glass transition temperatures well within the range of temperature excursions reached in typical TDTR and FDTR experiments [2,3], while the same is true for the denaturing temperature of proteins [4,5]. Whether the goal is to avoid such temperatures or investigate material properties at those temperatures, the calculation of the steady-state temperature rise due to laser heating is necessary.

In this study, we use the methodology developed in our previous work [6] to understand the steady-state temperature rise associated with semi-infinite substrates with both insulated and conductive (bidirectional heat flow from the surface) boundary conditions. We provide a MATLAB script for calculating the temperature rise for both pulsed and continuous wave (CW) laser sources with and without amplitude modulation[2]. Whereas our previous work [6] provided insight into the theoretical limitations of the thermal penetration depth from laser heating, our current study provides practical application to understand and control the steady-state temperature rise in pump–probe experiments. Therefore, we quantify the effects that various thermal length scales have on the steady-state temperature rise and generalize these results where appropriate. For a modulated heating event, these length scales include the $1/e^2$ pump radius (r_0), $1/e^2$ probe radius (r_1), and the thermal penetration depth, defined as the $1/e$ temperature decay length relative to the sample surface. In Ref. [6], we showed that the temperature rise resulting from a modulated heating event in TDTR and FDTR could be decoupled into a modulated and steady-state temperature response. As such, there are two thermal penetration depths to consider: the modulated thermal penetration depth (δ_m), which defines the $1/e$ decay in depth relative to the magnitude of the modulated component to temperature rise at the sample surface, and the steady-state thermal penetration depth (δ_s), which defines the $1/e$ decay in depth relative to the steady-state surface temperature rise.

From these calculations, we report several key findings based on typical experimental conditions used in TDTR and FDTR. First, we find that conductive thin film transducer layers, such as aluminum (Al) and gold (Au) films ubiquitous in TDTR and FDTR, can significantly reduce the temperature rise by providing radial heat dissipation, leading to reductions in temperature rise of (in some cases) orders of magnitude compared to the same temperature rise without a transducer. Second, when sampling thin films, conductive substrates can likewise reduce this temperature

[1]Corresponding author.

Contributed by the Heat Transfer Division of ASME for publication in the JOURNAL OF HEAT TRANSFER. Manuscript received June 22, 2017; final manuscript received October 26, 2017; published online February 6, 2018. Assoc. Editor: Alan McGaughey.

[2]https://patrickehopkins.com/publications/

 Copyright © 2018 by ASME

Downloaded From: http://heattransfer.asmedigitalcollection.asme.org/ on 05/18/2018 Terms of Use: http://www.asme.org/about-asme/terms-of-use

by acting as heat sinks. However, we find that their effectiveness as heat sinks is entirely dependent on the length of δ_s ($\approx r_0$) with respect to the film thickness. Third, we find that in bidirectional heat flow geometries [7], a substrate transparent to pump and probe wavelengths can greatly reduce the steady-state temperature rise; however, this substrate's thermal properties can dominate the modulated temperature response of the system so that sensitivity to other parameters is lowered considerably. Finally, we consider the effect of optical absorption by including an optical penetration depth (OPD), ζ, in our temperature rise calculations. We find that large ζ can reduce the steady-state temperature rise, but is only significant when it approaches the important thermal length scales such that $\zeta \approx \delta_s \approx r_0$. Taken together, this study emphasizes the need to decouple the modulated heating event from the steady-state heating event when considering laser heating and the importance of accurately determining the steady-state temperature rise for layered structures.

2 Results and Discussion

2.1 Theoretical Temperature Rise Profiles. We determine the temperature rise and heat flux for layered films using the solution to the radially symmetric heat diffusion equation, whereby the thermal properties of individual layers and interfaces are represented by matrices with hyperbolic decay terms [8–11]. In TDTR and FDTR, a laser is used as a heat source; upon absorption of the laser energy, a steady-state temperature profile is established in the material resulting from an energy balance of the laser heat flux absorbed on the sample surface and the dissipating heat flux into the sample. The temperature rise associated with a modulated laser heating source, whether the source is pulsed or CW, can be decoupled into a steady-state response resulting from the average power absorbed and a modulated response resulting from oscillations at the modulation frequency about the average power [6]. In the pulsed case, the steady-state response is taken as the accumulated temperature rise resulting from a summation over all pulses absorbed by the sample. For high repetition-rate lasers typically used in TDTR, the temperature rise associated with a single pulse is small compared to the accumulated temperature rise for low thermal conductivity materials where steady-state heating is of concern [6]. Additionally, the pulsed solution to steady-state heating, for the time-scales of interest in TDTR (100's of ps to several ns), can be approximated as a CW solution without significant loss of accuracy [6]. Thus, in this work, we generalize all results to hold true for both high-repetition rate pulsed and CW sources, but solve all temperature profiles assuming the heating event is from a CW source. Doing so has two advantages: (i) it is far more computationally efficient since summation over harmonics of the repetition rate is not required, and (ii) it eliminates any time dependence (however small) to the temperature profile between pulse absorption.

Although the temperature rise can be decoupled into two terms for the modulated laser heating event, in general, the steady-state temperature rise dominates the total temperature profile. The modulated temperature rise oscillates about the steady-state temperature such that when time-averaged over several periods it is zero. Moreover, for typical modulation frequencies used in TDTR and FDTR, the amplitude of the modulated temperature rise can be orders of magnitude lower than steady-state temperature rise. For example, Fig. 1 shows the steady-state and modulated temperature profiles associated with a representative 100 nm aluminum (Al) film on an amorphous silicon dioxide (a-SiO_2) substrate subjected to laser irradiation modulated at 10 MHz and absorbed at the Al surface. The average absorbed power is 1 mW and the beam has a Gaussian radial profile with a $1/e^2$ heater radius, $r_0 = 15$ μm. Figure 1(*a*) shows that the maximum temperature rise of the steady-state component is over 10 K. In contrast, Fig. 1(*b*) shows that the magnitude (amplitude of the temperature oscillation in time) of the modulated component of the temperature rise

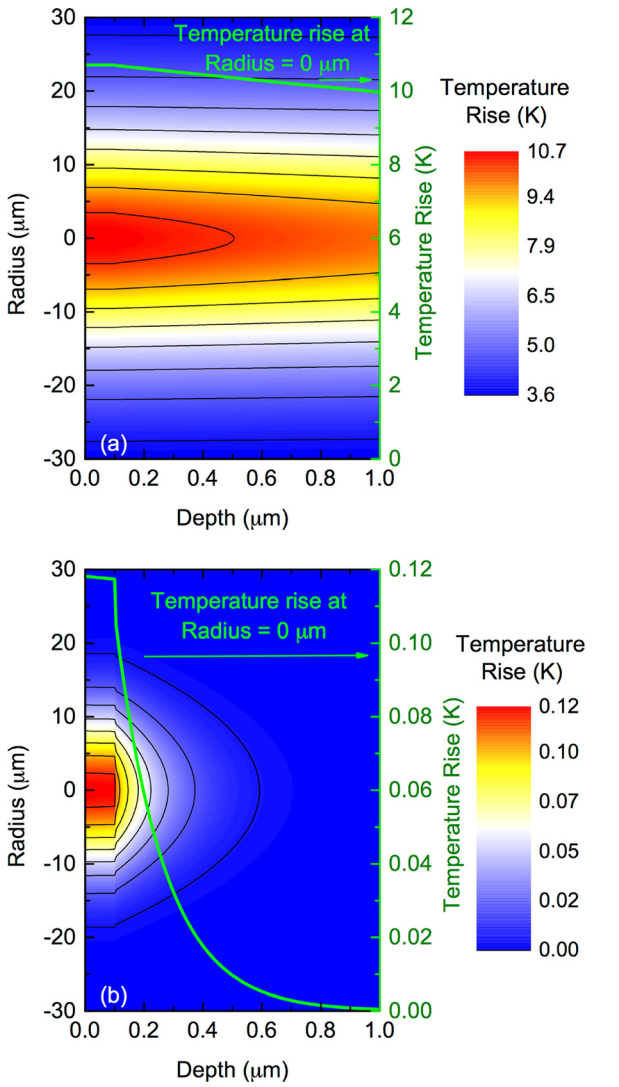

Fig. 1 Temperature profile as a function of radius and depth for a 100 nm Al/a-SiO_2 sample subjected to a radially symmetric Gaussian surface heating event with $1/e^2$ radius of 15 μm and an average absorbed power of 1 mW. The heating event is modulated sinusoidally at 10 MHz; the temperature profile is decoupled to display the (*a*) constant component from the unmodulated (steady-state) response and (*b*) the magnitude of temperature rise from the modulated component.

is two orders of magnitude lower than the steady-state component. The material-dependent thermal parameters used for the calculations shown in Fig. 1 (along with all other parameters used throughout the rest of the work) are listed in Table 1. Although this paper is focused on interpreting temperature profiles associated with TDTR and FDTR, most of the results presented in this study can be generalized to interpret temperature profiles associated with other experiments having radially symmetric heating at comparable length scales to those presented in this study.

The condition that $\delta_m \ll \delta_s$ is beneficial for determining thermal properties at a specific temperature in TDTR and FDTR. Since the depth of the experimental volume is typically assumed as δ_m [23,24], the condition of $\delta_m \ll \delta_s$ implies that we can assume a single temperature approximation within the experimental depth to avoid complications with spatially varying thermal properties. This approximation is important because, in order to extract thermal parameters via a heat diffusion model, fixed input parameters need to be defined; these parameters are generally temperature dependent. A single temperature approximation allows us to assign spatially invariant values to these fixed

Downloaded From: http://heattransfer.asmedigitalcollection.asme.org/ on 05/18/2018 Terms of Use: http://www.asme.org/about-asme/terms-of-use

Table 1 Room temperature thermal parameters used in calculating temperature rises in this study. κ_r is thermal conductivity in the radial (in-plane) direction, κ_z is thermal conductivity in the z (out-of-plane) direction, C_v is volumetric heat capacity, and $h_{Al(Au)/x}$ is the thermal boundary conductance between Al(Au) and the material of interest.

Material	κ_z (W m^{-1} K^{-1})	κ_r (W m^{-1} K^{-1})	C_v (J cm^{-3} K^{-1})	$h_{Al/x}$ (MW m^{-2} K^{-1})	$h_{Au/x}$ (MW m^{-2} K^{-1})
Air	0.026 [12]	0.026 [12]	0.0012 [12]	0.001 [12]	—
C_{60}	0.097 [13]	0.097 [13]	1.3 [13]	100[a]	—
Polymer	0.2 [14]	0.2 [14]	2.0 [14]	26 [15]	—
a-Si	1.3[b]	1.3[b]	1.62 [16]	100[a]	—
a-SiO_2	1.4 [17]	1.4 [17]	1.62 [16]	100[a]	50[c]
c-SiO_2[d]	12 [18]	6.8 [18]	1.62 [16]	180[c]	—
Al_2O_3[d]	35[c]	33	3.06 [16]	200 [19]	—
Si	140 [16]	140 [16]	1.65 [16]	100 [20]	—
Al	135[a]	135[e]	2.42 [21]	∞	—
Au	220[a]	220[e]	2.49 [21]	—	∞

[a]Estimated value; in practice this does not play a significant role in the temperature rise calculation.
[b]The thermal conductivity of a-Si has been shown to exhibit size effects [17] such that its bulk value is not well known; however, to comply with Ref. [22], we choose to model it with a fixed value of 1.3 W/m K.
[c]Measured with TDTR.
[d]z is assumed to be parallel to c-axis and r is perpendicular to c-axis.
[e]Measured using four-point probe resistivity and applying the Wiedemann–Franz law.

parameters. In Fig. 1, δ_m is limited to less than 300 nm for the Al/SiO_2 sample (including the 100 nm Al film thickness). The 99% temperature decay depth in this case is roughly 850 nm. Across the same depth, the temperature decay of the steady-state temperature is less than 10%, validating the assumption that the steady-state temperature rise is constant across the experimental depth. Increasing the modulation frequency or increasing the heater radius can further reduce the ratio of δ_m/δ_s, ensuring a single temperature approximation holds in depth.

The radial temperature decay lengths at the sample surface, on the other hand, are similar in the modulated and steady-state cases. To determine the conditions for which a single temperature approximation is valid in the radial direction, it is necessary to discuss the probe detection. When there is negligible depth in the probe optical absorption profile, the probe-averaged temperature rise (T_{PA}), to which the probe reflectivity is proportional, is defined by [10]

$$T_{PA} = \frac{4}{r_1^2}\int_0^\infty T_{top}\exp\left(\frac{-2r^2}{r_1^2}\right) r\,dr \tag{1}$$

where T_{top} is the surface temperature rise induced by the pump beam. For a bulk material, this expression can be solved analytically for an unmodulated CW source to become

$$T = \frac{\alpha A}{\sqrt{2\pi\kappa_r\kappa_z\left(r_0^2 + r_1^2\right)}} \tag{2}$$

where αA is the absorbed average power of incident laser irradiation. For an isotropic bulk material with thermal conductivity κ and when $r_1 = r_0$, this becomes [10]

$$T = \frac{\alpha A}{2\sqrt{\pi} r_0 \kappa} \tag{3}$$

This expression is often employed as an estimation of the steady-state temperature when pump and probe radii are similar, as it provides a simple analytical expression for calculating the temperature rise from laser heating. However, there are two assumptions inherent in Eq. (3) that complicate its use for TDTR and FDTR experiments when experimental conditions deviate from these assumptions.

The first assumption is that the radial distribution of temperature is accurately approximated by a single temperature coming from T_{PA} when $r_0 = r_1$. T_{PA} is a Gaussian average of the radial temperature distribution over the probe radius, providing a single temperature to estimate the radial decay of temperature for a sample. This means that in the case of large radial temperature gradients, Eq. (3) will significantly underestimate the maximum temperature of the system and the use of a single temperature approximation within the experimental volume of TDTR and FDTR may not be valid. For example, Fig. 2(*a*) shows the surface steady-state temperature profile induced by a pump beam with $r_0 = 15$ μm and $\alpha A = 1$ mW for a bulk a-SiO_2 sample assuming a surface heating event. When $r_1 = r_0$, the calculated temperature rise (T_{PA}), which agrees perfectly with Eq. (3), is only capturing the temperature rise associated with a fraction of the radial temperature gradient. When r_1 is reduced relative to r_0, T_{PA} changes significantly, as depicted in Fig. 2(*a*), approaching the peak temperature as $r_1 \to 0$ μm. While this simple example shows temperature deviations of only a few Kelvin, higher heat fluxes or lower thermal conductivity materials can greatly increase the steady-state temperature rise; we explore the latter case below. Before doing so, we generalize these results in Fig. 2(*b*), which shows the normalized temperature, defined as the ratio of maximum

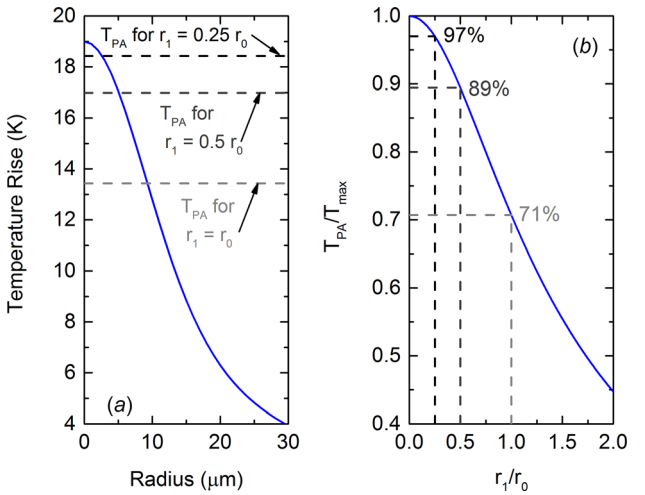

Fig. 2 (*a*) Temperature rise due to pump beam heating as a function of radius. T_{PA} is the probe-averaged temperature rise, shown for the cases when the probe radius is equal to pump radius, half the pump radius, and a quarter of the pump radius. (*b*) Normalized temperature (defined as probe averaged temperature rise divided by maximum temperature rise from pump heating) as a function of normalized probe radius (defined as the ratio of probe to pump radii).

Downloaded From: http://heattransfer.asmedigitalcollection.asme.org/ on 05/18/2018 Terms of Use: http://www.asme.org/about-asme/terms-of-use

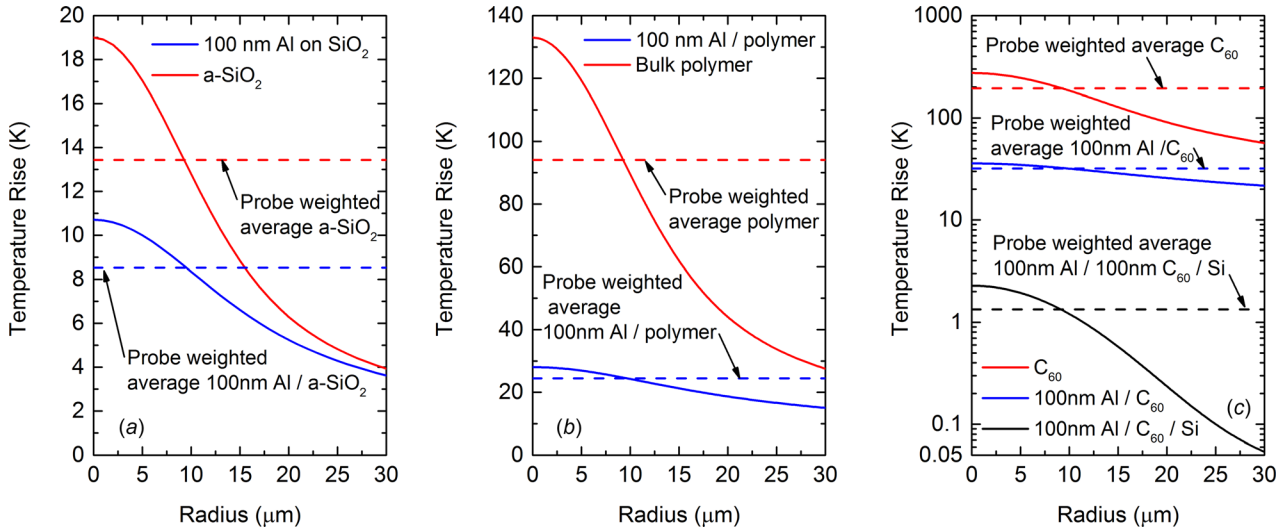

Fig. 3 Steady-state temperature rise as a function of radius for (*a*) bulk amorphous SiO_2 and a 100 nm Al film on a SiO_2 substrate, (*b*) bulk polymer and a 100 nm Al film on a polymer substrate, and (*c*) bulk disordered C_{60}, a 100 nm Al film on a C_{60} substrate, and a 100 nm Al film on a 100 nm C_{60} film on a Si substrate

temperature of the radial surface temperature profile (T_{max}) to T_{PA}, as a function of normalized probe radius (r_1/r_0). When the normalized radius is 1, T_{PA} gives a temperature of 71% of the maximum temperature, while lowering the normalized radius to 0.5 and 0.25 increases the normalized temperature rise to 89% and 97%, respectively. These results are independent of laser power and material properties for this bulk, homogeneous case, allowing for a generalized understanding of the conditions needed ensure a single temperature approximation in the radial direction. Since the radial component to the measurement volume is dictated by the probe, it is beneficial to reduce the probe radius relative to the pump radius to ensure a single-temperature approximation in the radial direction.

The second assumption in Eq. (3) is that the sample is bulk and homogeneous, which is not valid when layers and interfaces are considered. Since TDTR and FDTR experiments almost always require a thin-film metal transducer layer, Eq. (3) becomes invalid. To show this, in Fig. 3, we consider the steady-state surface temperature profiles for three representative low-thermal conductivity materials (*a*) a-SiO_2, (*b*) polymer, and (*c*) disordered C_{60}. In all cases, a surface heating event with $r_0 = 15$ μm and $\alpha A = 1$ mW is used and all temperature profiles are shown with and without a 100 nm Al transducer layer (typical thickness used in TDTR and FDTR). Additionally, T_{PA} is shown to demonstrate the equivalence of Eq. (3) and T_{PA} when $r_1 = r_0$ and no transducer layer is included. The addition of the transducer layer completely changes the steady-state temperature profile. For a-SiO_2, T_{max} is reduced by 44% with the addition of the transducer layer, while the difference is compounded in the case of polymers and C_{60}, reducing the peak temperature by 79% and 87%, respectively.

This strong temperature reduction occurs because the transducer acts as a heat sink in the radial direction. This radial heat sink effect is shown in Fig. 4 through the comparison of the heat flux vector field (which includes heat flux components in the depth and radial directions) for (*a*) bulk a-SiO_2 and (*b*) 100 nm Al on a-SiO_2. In these examples, $r_0 = 1$ μm to be comparable to the transducer thickness for better visualization of the heat flux in the Al layer. For bulk a-SiO_2, the heat flux is dissipated throughout the depth and radial directions with similar magnitudes. However, when a 100 nm Al layer is added, the radial heat flux in the Al layer is much greater than any magnitude of heat flux in the a-SiO_2 layer. In order to sustain the similar radial temperature

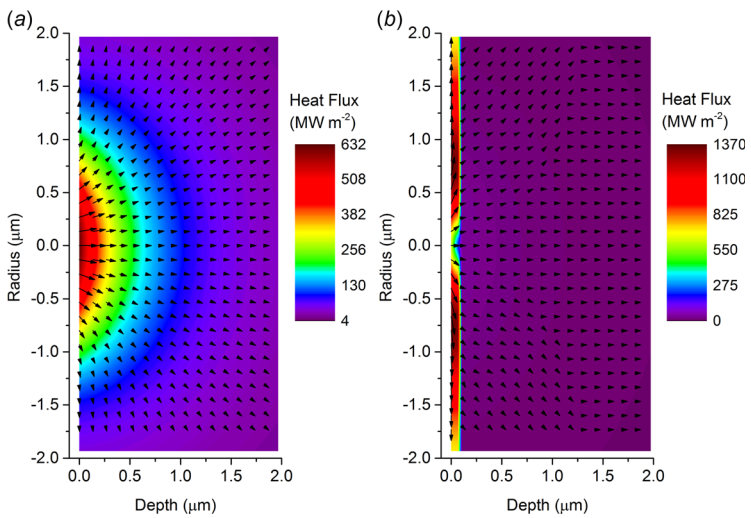

Fig. 4 Heat flux vector field resulting from steady-state heating in (*a*) bulk a-SiO_2 and (*b*) 100 nm Al on a-SiO_2 when $r_0 = 1$ μm and $\alpha A = 1$ mW. The magnitude of the heat flux is shown as a contour.

Downloaded From: http://heattransfer.asmedigitalcollection.asme.org/ on 05/18/2018 Terms of Use: http://www.asme.org/about-asme/terms-of-use

profiles in both the Al layer and a-SiO_2 (see Fig. 1), the radial heat flux in the Al must be much greater than that in the a-SiO_2 to compensate for the difference in thermal conductivities.

This heat sink effect is generally not a factor in the modulated temperature rise, emphasizing the need to decouple the steady-state and modulated temperature profiles that occur simultaneously with a modulated laser heating event. Whereas the latter can typically be assumed one-dimensional so that radial thermal transport is negligible, the former is highly dependent on radial transport. We quantify this further in an experimental case study on a thin Au film deposited on a-SiO_2 substrate in Sec. 2.2. Although the steady-state heating is partially mitigated by the transducer layer, when studying thin films, the use of a conductive substrate can further reduce the heating, as shown in Fig. 3(*c*), where the steady-state temperature rise is calculated for 100 nm Al on a C_{60} thin film with thickness $d = 100$ nm (a thickness achievable for spin-coated thin films) on a bulk Si substrate. In this case, the temperature rise, compared to bulk C_{60} alone, is reduced by two orders of magnitude.

This substrate heat sink is limited by the relative length scales of the film thickness and heater radius such that it is most effective when $d \ll r_0$. That is, when the thin film thickness approaches or surpasses the length scale of the heat source, the thin film thermal properties, rather than the substrate properties, dictate the temperature response of the sample. To illustrate this, we again consider a thin film of disordered C_{60} on Si and a-SiO_2 substrates. Shown in Fig. 5(*a*) is the ratio of the surface temperature rise calculated for a thin film of disordered C_{60} on a substrate to that of bulk C_{60} (T_{film}/T_{bulk}), as a function of C_{60} film thickness divided by heater radius (d/r_0). For all calculations, the pump and probe radii are equal. As d/r_0 becomes larger, the temperature rise for the thin film case approaches that of bulk C_{60}. On a silicon substrate, when $d/r_0 = 0.1$, the temperature rise is over 11% of T_{bulk}; at a ratio of 1, it is over 65%. Given that beam radii can be on the order of 1 μm for relatively high objective lens magnifications (e.g., 20× and higher), substantial heating can occur, even if a conductive substrate is used. However, in TDTR and FDTR, the transducer layer further dissipates this heat. Figure 5(*b*) shows the temperature rise of the same disordered C_{60} films on Si as in Fig. 5(*a*), now with a 100 nm Al transducer. In this case, the temperature rise is normalized by that of the 100 nm Al on bulk C_{60} case, since this is the maximum temperature rise achievable. As the C_{60} film thickness is increased, T_{film}/T_{bulk} approaches 1, similar to the situation shown in Fig. 5(*a*). However, the heater radius dictates when this transition to bulk occurs. In all cases, the substrate influence on temperature rise is limited by the relative length scales of heater to thin film. In fact, when the heater radius is small, the transducer layer can dissipate heat more effectively than the substrate.

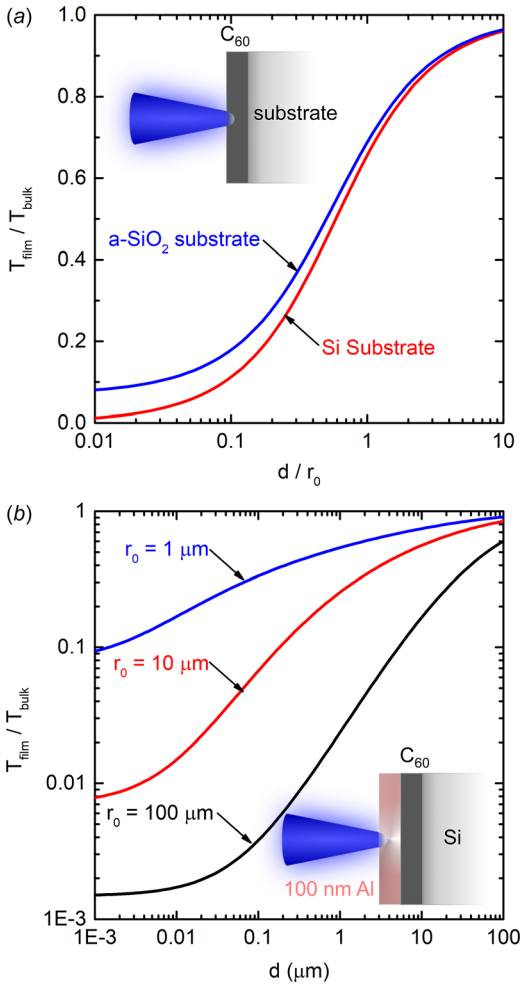

Fig. 5 (*a*) Ratio of the steady-state temperature rise for a thin film of disordered C_{60} on Si and SiO_2 (T_{film}) to that of bulk C_{60} (T_{bulk}) as a function of the ratio of C_{60} film thickness (d) to heater radius (r_0). (*b*) Ratio of the steady-state temperature rise for 100 nm Al on a thin film of disordered C_{60} on Si (T_{film}) to that of 100 nm Al on bulk C_{60} (T_{bulk}) as a function of C_{60} thickness (d). In all cases, $r_1 = r_0$.

2.2 Experimental Case Study: Au on a-SiO_2. To validate the calculations of steady-state heating, provide an example of when properly estimating temperature rise is important, and develop an iterative approach to determining temperature-dependent thermal properties, we study the case of a-SiO_2 with a nominal 65 nm gold (Au) transducer layer using TDTR, the details and analyses for which are described elsewhere [10,25,26]. Gold was chosen as the transducer because of its high absorbance at our pump wavelength of 400 nm, which allows for large steady-state temperature rises. Additionally, Au has low absorbance at the probe wavelength of 800 nm, so we can ignore any contribution by the probe when calculating the steady-state temperature rise. An a-SiO_2 substrate was chosen because of its well-established thermal conductivity as a function of temperature, making it a good choice for proof of concept. We measure the ratio of the in-phase to out-of-phase voltage of the probe response recorded by a lock-in amplifier as a function of probe delay time. The $1/e^2$ radii for the pump and probe are 16.5 and 6.5 μm, respectively. The pump pulses are modulated with a 10 MHz sinusoidally varying envelope. Using a high modulation frequency and small probe radius relative to the pump ensure the single temperature approximation will be reasonably accurate for our experimental volume, as discussed in Sec. 2.1. Using a multilayer, radially symmetric thermal model [10,26], we fit for the thermal boundary conductance between the Au transducer and the a-SiO_2 ($h_{Au/a\text{-}SiO_2}$) and the a-SiO_2 thermal conductivity ($\kappa_{a\text{-}SiO_2}$). We assume bulk values for the heat capacities [16,21] for the Au transducer and a-SiO_2 and adjust these with temperature as appropriate. The radial component to thermal conductivity of the Au transducer is determined using the Wiedemann–Franz law based on 4-point probe resistivity measurements.

To elucidate the importance of the thermal parameters that determine the temperature rise (both modulated and steady-state), we quantify the sensitivity of the surface temperature response function to each parameter of interest as described by [27]

$$S_p = \frac{\partial \ln(V)}{\partial \ln(p)} \tag{4}$$

where V is response function of interest, in this case the magnitude of the in-phase and out-of-phase temperature response, and p is the parameter of interest. Although we fit for the ratio of in-phase to out-of-phase signals to improve the signal-to-noise ratio, to

Downloaded From: http://heattransfer.asmedigitalcollection.asme.org/ on 05/18/2018 Terms of Use: http://www.asme.org/about-asme/terms-of-use

theoretically compare the modulated and steady-state responses, the magnitude is used since the steady-state response has no out-of-phase component. Figure 6(*a*) shows the sensitivity of the 10 MHz modulated component of temperature rise, while Fig. 6(*b*) shows the sensitivity of the steady-state component. In both cases, higher absolute value of sensitivity indicates greater importance of a parameter to the temperature response function. Comparison of the two suggests that in the modulated case, the influence of both in-plane and cross-plane thermal conductivities of the Au layer ($\kappa_{Au,r}$ and $\kappa_{Au,z}$, respectively) is negligible to the magnitude of the temperature response. In contrast, the heat capacity ($C_{v,Au}$) and, by extension, the thickness of the Au film (d_{Au}) play critical roles in determining this response. As expected, the radial component to the thermal conductivity of a-SiO_2 ($\kappa_{a\text{-}SiO_2,r}$) has a negligible sensitivity to the temperature rise since the decay length in depth is much smaller than that radially such that heat flow is essentially one-dimensional. Because at typical TDTR modulation frequencies the thermal effusivity dominates the modulated temperature response from the a-SiO_2 [28], the heat capacity ($C_{v,a\text{-}SiO_2}$), and cross-plane thermal conductivity ($\kappa_{a\text{-}SiO_2,z}$) are indistinguishable and share the same sensitivity. Finally, the thermal boundary conductance between Au and a-SiO_2 ($h_{Au/a\text{-}SiO_2}$) has a significant contribution to the modulated temperature response due to the relatively low measured value of $\sim$50 W m^{-2} K^{-1}, which could be due to poor adhesion between the substrate and metal film [29,30]. Taken together, the important parameters in determining the modulated temperature response function are temperature dependent. In particular, $C_{v,Au}$ is crucial for accurately determining the modulated temperature response. When analyzing TDTR data, we fit for $\kappa_{a\text{-}SiO_2,z}$ and $h_{Au/a\text{-}SiO_2}$. However, it is essential to input appropriate estimates for $C_{v,Au}$ and $C_{v,a\text{-}SiO_2}$ based on steady-state temperature rise calculations to accurately determine the thermal properties of interest. Thus, we need to understand the sensitivity of the steady-state temperature response to these parameters.

The steady-state temperature response sensitivity to the same parameters is shown in Fig. 6(*b*). In contrast to the modulated sensitivities, the heat capacities and thermal boundary conductance are negligible, whereas the thermal conductivities (apart from $\kappa_{Au,z}$) dictate the temperature rise. The sensitivity to $\kappa_{Au,z}$ is negligible due to the limited thickness of the Au layer relative to the thermal penetration depth of the steady-state temperature profile. Therefore, as previously alluded to, the length and time-scales of the temperature decay dictate the importance of the thermal parameters to the temperature response at the surface. In TDTR, this means that estimating the temperature rise governing the thermal parameters involves an appropriate estimation of the steady-state temperature rise. However, this temperature rise is governed by the thermal conductivity of the material of interest, which is often the desired property to be measured in TDTR experiments.

To overcome this conflict and demonstrate a practical approach to employ temperature rise calculations in conjunction with TDTR, we simultaneously estimate the steady-state temperature rise and fit the a-SiO_2 thermal conductivity iteratively via the process described in the inset of Fig. 7. The laser power was measured and the Au absorbance was assumed to be 0.606 [32]. Starting with the phase-corrected TDTR ratio data, we (1) input thermal parameters based on a lookup table of thermal properties versus temperature, interpolating where necessary. We then (2) fit the thermal model governing the modulated surface temperature response to the TDTR data to extract $\kappa_{a\text{-}SiO_2,z}$ and $h_{Au/a\text{-}SiO_2}$. These values, along with the other thermal parameters, are then used to (3) calculate the steady-state temperature rise based on the full solution to the heat diffusion equation for a layered sample. We then return to step (1) to repeat the process until a convergence of temperature is reached. In this case, it took only five iterations on average to reach a convergence. To emphasize the importance of the transducer layer to the steady-state temperature rise calculation, we perform this iterative method in two ways: calculating temperature rise with and without the transducer layer. Note that the fit always includes the transducer layer and only the steady-state temperature rise calculation is altered.

Figure 7 shows the resulting converged temperature rises and fitted thermal conductivities for both cases of including and not including the transducer when calculating the steady-state temperature rises. Uncertainties correspond to statistical variations between measurements as well as uncertainty in Au film thickness

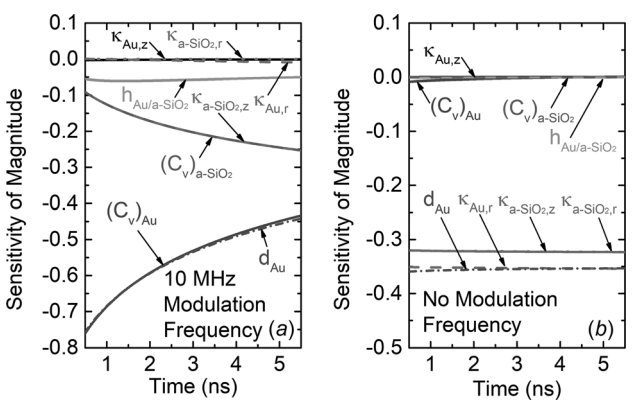

Fig. 6 Sensitivity of the magnitude of surface temperature rise to thermal parameters as determined by Eq. (4) for the (*a*) 10 MHz modulated frequency response and (*b*) steady-state unmodulated response for a 65-nm Au on a-SiO_2 sample. Thermal parameters considered include in-plane and cross-plane thermal conductivities (κ_r and κ_z, respectively) for both the Au and a-SiO_2 layers, volumetric heat capacities (C_v) for both layers, and thermal boundary conductance across the Au/a-SiO_2 interface ($h_{Au/a\text{-}SiO_2}$).

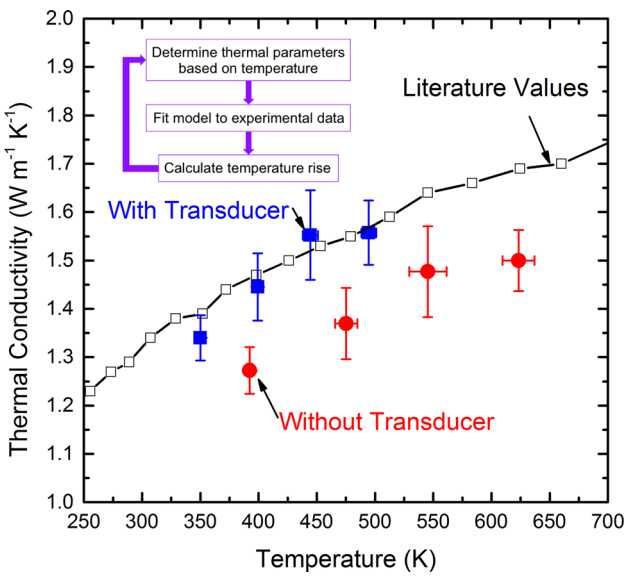

Fig. 7 Experimentally determined thermal conductivities of a-SiO_2 measured with TDTR when a 65 nm Au transducer layer is used. Solid squares denote the fitted values with temperatures based on calculations that include the Au transducer layer, while solid circles denote the fitted values using temperature rise calculations without including the Au transducer. In both cases, an iterative method was used as described by the inset, whereby input thermal parameters were chosen based on the steady-state temperature rise calculated, the TDTR data were used to fit the a-SiO_2 thermal conductivity and the Au/a-SiO_2 thermal boundary conductance, and all thermal parameters were then used to recalculate the steady-state temperature rise. This process is repeated until convergence is reached. Literature values are taken from Ref. [31].

Downloaded From: http://heattransfer.asmedigitalcollection.asme.org/ on 05/18/2018 Terms of Use: http://www.asme.org/about-asme/terms-of-use

(measured via mechanical profilometry as 63–65 nm). The latter, because it is coupled to the heat capacity through the thermal mass of the film so that they share similar sensitivities, is the largest contribution to the uncertainty. A comparison of the measured values of thermal conductivities to literature values [31] shows that the measured values, when performing the appropriate temperature rise calculations, agree well with literature values. In contrast, not accounting for the transducer results in an overprediction of the temperature rise so that C_{v,SiO_2} is overestimated. Due to the coupling of $C_{v,a\text{-}SiO_2}$ and $\kappa_{a\text{-}SiO_2,z}$ in this thermal effusivity regime, $\kappa_{a\text{-}SiO_2,z}$ is underpredicted, resulting in a disagreement with literature values.

3 Heat Dissipation Methods and Bidirectional Heat Flow Geometries

It is clear that the steady-state temperature rise can be large in experiments. However, the previous discussion has alluded to methods of mitigating this temperature rise. Namely, a metal transducer layer, in addition to providing surface absorption and high reflectivity that are beneficial to performing optical thermometry, provides a radial heat sink that can significantly reduce the steady-state temperature rise. The use of a conductive substrate, such as silicon, can greatly reduce the heating as well, but is only applicable for thin films. Adding such a heat sink to a bulk material will not mediate heat dissipation until the heater size is comparable to the thickness of the film of interest. Another approach to heat dissipation involves the use of a sample geometry supporting bidirectional heat flow. Such a geometry consists of a sample of interest in contact with a metal transducer, but adjacent to the metal surface (plane of laser absorption) is a transparent substrate through which the pump and probe beams traverse. These geometries are commonly used in TDTR and FDTR to study thermal properties of porous materials and liquids and to understand energy transport across solid/liquid interfaces [7,33–37].

In such bidirectional heat flow geometries, the thermal energy will dissipate into the transparent substrate side and sample side based on the collective material and interfacial properties of both sides. If one side is much more conductive than the other, heat will flow through the conductive side to maintain symmetry in the steady-state temperature rise about the plane of laser absorption [6]. Thus, the temperature can be greatly reduced relative to the insulated case previously discussed. To quantify this temperature reduction, in Fig. 8, we show the same polymer sample considered in Fig. 3(*b*) configured to support bidirectional heat flow geometry. The sample is (from left to right) transparent substrate/100 nm Al/polymer. The transparent substrate is varied between materials ranging from highly thermally conductive (Si) to highly insulating (air). These calculations assume that the pump and probe wavelengths can be chosen such that these substrates are transparent. The temperature rise profile for two such transparent substrates is shown in Fig. 8 for (*a*) Al_2O_3 and (*b*) a-SiO_2 for the same conditions ($r_0 = 15$ μm and $\alpha A = 1$ mW) used in previous calculations. The contour plot of temperature rise in the case of Al_2O_3 reveals a reduction in maximum temperature by about 97% compared to the insulated case previously discussed; SiO_2, despite its relatively lower thermal conductivity, also serves to reduce the peak temperature by 65%. The magnitude of the 10 MHz modulated component of temperature rise at $r = 0$ μm is also shown to compare the relative temperature rises and decay lengths of interest to TDTR/FDTR experiments. Finally, Fig. 8(*c*) displays a summary of the surface temperature distribution across the radial direction for all transparent substrates considered, which include air, polymer, a-SiO_2, quartz (c-SiO_2), Al_2O_3, and Si. We note that the radial heat conduction in the Al thin film is still a prominent source of heat dissipation in this bidirectional heat flow geometry. In fact, the reduction in peak surface temperature with an identical polymer layer as the transparent substrate is reduced by ~25% rather than 50% because the dominant heat sink is still the Al film. However, if we remove the transducer layer, such that a bulk polymer is in contact with a transparent polymer, the steady-state temperature rise is reduced by the expected 50% compared to the insulated bulk polymer case, from a peak temperature of 133 K to 66.5 K, resulting from symmetry in heat flux throughout either side.

From this study on the variation of substrates, it is clear that the parallel heat flow geometry provides an additional method of heat dissipation. However, it comes at a cost to TDTR/FDTR experiments; since heat flows preferentially to the most conductive channel, sensitivity to thermal parameters of interest within the insulating channel can be low. Consider the same transparent substrate/100 nm Al/polymer sample—if the thermal conductivity of the polymer is the fitting parameter of interest—one must ensure that enough heat is still channeled into the polymer layer to allow for the thermal model to become sensitive to that parameter.

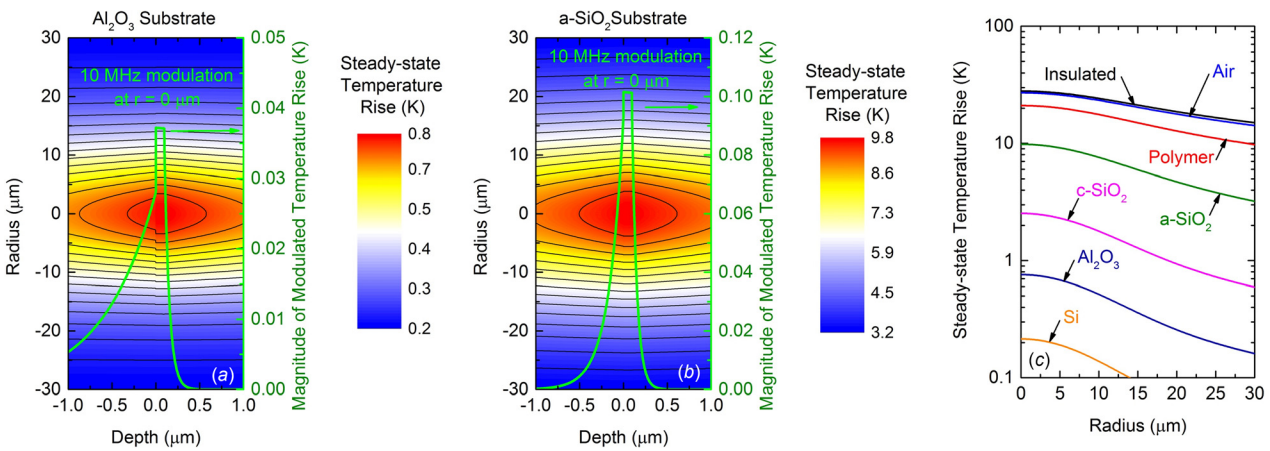

Fig. 8 Temperature distributions for the bidirectional heat flow geometry consisting of transparent substrate/100 nm Al/polymer where laser irradiation occurs at the Al surface adjacent to the transparent substrate. For the case of this transparent substrate being (*a*) Al_2O_3 and (*b*) SiO_2, the steady-state (unmodulated) temperature profile is displayed as a contour in radius and depth, while the solid line is the magnitude of modulated temperature at $r = 0$ μm for a modulation frequency of 10 MHz. In both cases, positive depth depicts the Al/polymer side, while negative depth depicts the transparent substrate side. (*c*) depicts the steady-state surface temperature rise for the same bidirectional heat flow geometry where the transparent substrate is varied to span a wide range of thermal conductivities from Si (140 W m^{-1} K^{-1}) to complete insulation. All thermal parameters used for these calculations are listed in Table 1.

Downloaded From: http://heattransfer.asmedigitalcollection.asme.org/ on 05/18/2018 Terms of Use: http://www.asme.org/about-asme/terms-of-use

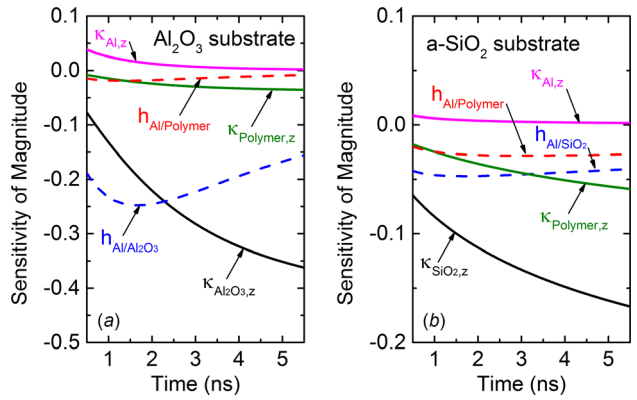

Fig. 9 Sensitivity of the magnitude of modulated surface temperature rise (10 MHz modulation frequency) to thermal parameters as determined by Eq. (4) for the (*a*) Al_2O_3/100 nm Al/polymer and (*b*) a-SiO_2/100 nm Al/polymer in the case of laser irradiation at the Al surface adjacent to Al_2O_3 (a-SiO_2). Thermal parameters considered include cross-plane thermal conductivities (κ_z) for Al, Al_2O_3 (a-SiO_2), and polymer layers and thermal boundary conductances across the Al/Al_2O_3 (SiO_2) interface ($h_{Al/Al_2O_3(a\text{-}SiO_2)}$) and across the Al/polymer interface ($h_{Al/polymer}$).

Figure 9 shows the sensitivity to thermal conductivities and thermal boundary conductances associated with this sample when the transparent substrate is (*a*) Al_2O_3 and (*b*) a-SiO_2 using the same pump and probe radii used in Fig. 6. In the former case, the magnitude of the modulated temperature response is overwhelmingly sensitive to properties of the Al_2O_3 side, including its cross-plane thermal conductivity $\kappa_{Al_2O_3,z}$ and thermal boundary conductance with Al (h_{Al/Al_2O_3}). By comparison, the thermal properties of the Al/polymer side, including Al and polymer thermal conductivities ($\kappa_{Al,z}$ and $\kappa_{polymer,z}$) and thermal boundary conductance (h_{Al/Al_2O_3}), have a smaller influence on the temperature response, which means that it may not possible to accurately determine these parameters with acceptable uncertainty. Note that radial thermal conductivities are not considered here since heat flow is one-dimensional due to a large pump radius relative to the thermal penetration depth for this modulated heating event, similar to the case of an insulated boundary condition previously discussed. If the transparent substrate is changed from Al_2O_3 to a-SiO_2, the sensitivity to $\kappa_{polymer,z}$ is increased significantly relative to the thermal properties on the a-SiO_2 side. While the sensitivity to $\kappa_{a\text{-}SiO_2,z}$ is still large, the sensitivity to $\kappa_{polymer,z}$ is enough to determine this parameter with confidence, since a-SiO_2 is a well-studied material having little variation in thermal conductivity. These findings suggest that lowering the substrate thermal conductivity enhances sensitivity to the insulating layer thermal conductivity. However, since steady-state temperature mitigation is of concern, one must find the appropriate balance between this temperature mitigation and sensitivity to thermal parameters of interest; this will ultimately come down to the uncertainty of fixed input parameters for the thermal model and the tolerance for uncertainty in the fitting parameters. Changing experimental parameters like pump radius or modulation frequency may also improve sensitivity to fitting parameters.

4 Consideration of Depth-Dependent Optical Absorption

Recent works have demonstrated the ability to use TDTR/FDTR to measure materials without the use of a thin-film transducer layer [22,38]. For this purpose, the effects of optical absorption- and depth-dependent laser excitation must be considered. To incorporate these effects into our model for both the steady-state and modulated temperature rises, the laser heating is treated as a source term, rather than a boundary condition, in the heat diffusion equation. As such, the source term for a bulk sample is described by [22,38]

$$S(z,r,t) = \frac{2\exp\left(-\frac{2r^2}{r_0^2}\right)\exp\left(-\frac{z}{\zeta}\right)G(t)}{\pi r_0^2 \zeta} \tag{5}$$

where ζ is the OPD of the absorbing layer and $G(t)$ is a function describing the time variation of the laser heating event; altering $G(t)$ allows for the description of modulation and pulses. Using this approach, we calculate the steady-state temperature rise and heat flux profiles for a bulk amorphous Si (a-Si) sample with OPD of 300 nm [22] for the pump wavelength in FDTR. To understand the effect of this parameter on the temperature profile, we also vary the OPD from 0 to 15 μm (the pump spot size) and calculate the variation in maximum temperature. The results are summarized in Fig. 10, where the (*a*) steady-state temperature and (*b*) heat flux profiles are shown for a-Si irradiated by a pump laser with $r_0 = 15$ μm and $\alpha A = 1$ mW. In this case, because the insulated boundary condition is invoked, there is no depth component

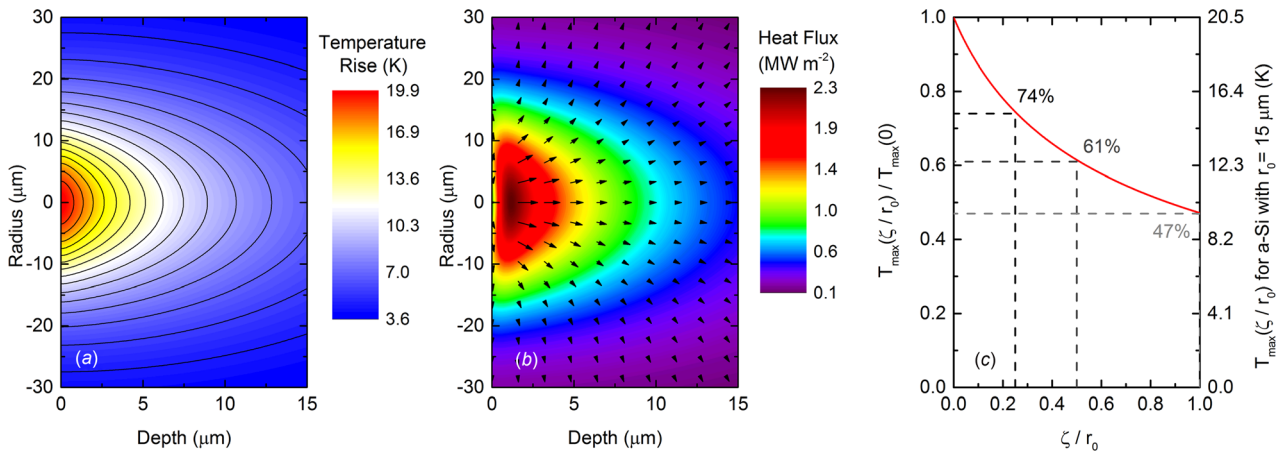

Fig. 10 Effect of optical penetration depth on the heating of bulk materials: (*a*) and (*b*) depict the steady-state temperature profile and heat flux for a bulk a-Si film when $r_0 = 15$ μm and $\alpha A = 1$ mW and the optical penetration depth is 300 nm. (*c*) Maximum temperature rise for the same sample. The normalized temperature, defined as the ratio of maximum temperature with a finite optical absorption depth to the maximum temperature assuming all optical absorption occurs at the surface, is also plotted as a function of normalized optical penetration depth, defined as the ratio of optical penetration depth to pump radius.

Downloaded From: http://heattransfer.asmedigitalcollection.asme.org/ on 05/18/2018 Terms of Use: http://www.asme.org/about-asme/terms-of-use

to heat flux at the surface, which results in a shifted distribution of heat flux compared to the surface boundary condition applied throughout Secs. 2–4. However, the temperature is still maximum at the surface; the influence of depth-dependent optical absorption is to reduce this maximum temperature by distributing the heat flux into the depth of the sample. A comparison of this temperature distribution to the same surface heating event ($\zeta = 0$) reveals little difference between them. The maximum temperature is reduced in the former case by less than 3%, a clear reduction but not likely to be of consequence to pump–probe experiments when estimating the steady-state temperature rise.

As with all previous discussion on the steady-state temperature rise, we emphasize the importance of length scales when generalizing these results. Although the influence of a 300 nm optical penetration depth has a negligible effect on the steady-state temperature profile of the bulk a-Si when a 15 μm pump radius is used, as ζ is increased (or equivalently, r_0 is reduced), the role of ζ becomes more influential in determining the temperature rise. To quantify this, we show in Fig. 10(*c*) the difference in maximum temperature when ζ is varied from 0 to 15 μm. Moreover, we generalize these results, which for isotropic bulk materials prove to be independent of material properties and absorbed power when normalizing the temperature rise. We define the normalized maximum temperature as the ratio of maximum temperature when an optical penetration depth of ζ is used to the maximum temperature when all the laser power is absorbed at the surface such that $\zeta = 0$. The normalized OPD is defined by the ratio ζ/r_0. Thus, we have incorporated the important length scale of radius to demonstrate that when ζ/r_0 is small, the steady-state temperature rise can be calculated using a surface heating event without significant loss of accuracy. This also means that when considering the probe averaged temperature rise, Eq. (3) becomes a good estimation for the temperature rise when the pump and probe spot sizes are similar.

An important final note is that this discussion has been focused on the steady-state, rather than modulated, temperature rise. The 300-nm OPD proved to negligibly affect the steady-state temperature rise in the a-Si example above due to the length scale of temperature decay in both radius and depth being two orders of magnitude greater than this OPD. This is not the case for a modulated heating event detected in TDTR/FDTR, which typically has a thermal penetration depth on the order of 10's to 100's of nm for the low thermal conductivity materials discussed throughout this paper. As a result, the OPD plays a crucial role in the temperature response of the modulated heating event, as shown by Wang et al. [38] and Yang et al. [22]. In summary, when the optical penetration depth becomes on the order of the defining length scales of temperature decay, large deviations in temperature distributions can exist relative to the surface heating case.

5 Limitations and Final Discussion

There are several limitations to the methodology employed throughout this paper for calculating the steady-state temperature rise. One such limitation is that this model is only valid in the diffusive and continuum limit to heat transfer. Thus, at length scales when Fourier's law breaks down due to heat carrier length scales exceeding the experimental volume, this approach will not capture the temperature rise accurately within that volume [39,40] without adjusting the thermal properties to become "effective" properties rather than intrinsic. For such cases, other approaches such as solving the full Boltzmann transport equation may prove more appropriate. However, in most pump–probe techniques having beam radii on the order of >1 μm, steady-state heating is typically only a concern for materials with low thermal conductivities resulting from relatively short mean-free-path vibrations. Therefore, for most practical applications, a diffusive heat equation is valid for calculating the steady-state temperature rise. A similar complication can arise with the use of the exponential decay of heat flux described in Eq. (5). This term implicitly assumes that the heat carriers absorbing the optical energy thermalize with the same exponential decay in depth. This is not the case for materials with weak electron–phonon coupling (e.g., Au or Ag) or long carrier relaxation times.

Throughout this paper, we discuss the heating imposed by a pump beam in pump–probe techniques but have neglected the temperature rise associated with the heating due to the probe beam. Accounting for the temperature rise associated with the probe beam is necessary when the absorbed power density of the probe becomes significant compared to the pump. Doing so is no different than the calculation of temperature rise from the pump, and the total temperature rise is simply the addition of both pump and probe temperature rises, due to the property of superposition [25]. However, in typical experimental conditions, the probe contribution to temperature rise is often negligible due to the high reflectivity at probe wavelengths needed for thermoreflectance measurements and the low power needed to establish a measurable signal. For example, the probe power used in the experimental case study was only 3 mW while the pump was varied from 10 mW to 40 mW. To compound this discrepancy, we used a gold transducer layer, which has an absorbance of $\sim$0.6 for the 400 nm pump but less than 0.03 for the 800 nm probe. Thus, the absorbed powers are roughly 6–24 mW for the pump and only $\sim$0.1 mW for the probe. In this case, it is clear that the probe contributes negligibly to the steady-state temperature rise compared to the pump. However, given other transducers such as aluminum or platinum, or different wavelengths used for pump and probe, the probe may have a larger influence on the steady-state temperature rise.

Finally, there are limitations to the heat diffusion equation invoked here when large steady-state temperature gradients can exist in the in-plane and cross-plane directions. Since the thermal properties that determine these gradients are temperature dependent, the thermal properties can vary spatially such that nonlinear spatial temperature derivative terms arise in the heat diffusion equation. In many cases, such as for amorphous materials whose thermal conductivities vary negligibly around and above their Debye temperatures, these nonlinear terms can be ignored such that heat diffusion model used here is valid for determining the steady-state temperature rise. When this is not the case, one must account for the temperature-dependent properties throughout all spatial gradients, which significantly complicates the analysis. For such applications, finite difference methods or more rigorous analyses based on solving the Boltzmann transport equation may be more appropriate.

6 Conclusion

In conclusion, in this study, we calculated the steady-state temperature rise for typical pump–probe experimental conditions and showed the influence of this quantity on several technologically relevant materials. In TDTR and FDTR using metal transducer layers, the transducer layer acts as a radial heat sink when the sample of interest is thermally insulating. Thus, when accounting for the steady-state temperature rise, the role of this layer becomes important; in the examples described in this work, the temperature estimation varied by an order of magnitude when comparing the cases of including and ignoring a 100 nm Al layer. Furthermore, the use of a thermally conductive substrate can mitigate temperature accumulation in such materials, but only when the thermal penetration depth is on the order of the insulating film thickness. An alternative approach to heat dissipation is to incorporate a transparent substrate adjacent to the laser irradiated surface to allow for heat to flow in parallel to the sample and to the substrate. Doing so can reduce sensitivity to the sample properties in TDTR and FDTR, so it is important to find the appropriate balance between parameter sensitivity and temperature rise to optimize measurement capability. Finally, the inclusion of an optical penetration depth into these calculations reveals that this optical absorption skews the heat flux distribution away from the sample

Downloaded From: http://heattransfer.asmedigitalcollection.asme.org/ on 05/18/2018 Terms of Use: http://www.asme.org/about-asme/terms-of-use

surface to reduce the steady-state temperature rise overall. However, this is only of consequence when the optical penetration depth approaches the length scales of thermal decay, governed by the pump radius and thermal penetration depth.

Acknowledgment

J. L. B. was supported by the Department of Defense (DoD) through the National Defense Science and Engineering Graduate Fellowship (NDSEG) Program.

Funding Data

- Office of Naval Research (Grant Nos. N00014-15-1-2769 and N00014-15-1-2863).

Nomenclature

A = average laser power
C_v = volumetric heat capacity
d = thickness
$h_{X/Y}$ = thermal boundary conductance between material X and Y
r_0 = $1/e^2$ pump radius
r_1 = $1/e^2$ probe radius
S_p = sensitivity to experimental parameter p
T = change in temperature relative to the reference temperature
T_{PA} = probe-averaged surface temperature rise
α = absorbance
δ_m = thermal penetration depth for the magnitude of the modulated temperature profile
δ_s = thermal penetration depth for the steady-state temperature profile
ζ = optical penetration depth
κ_r = thermal conductivity in the radial (through-plane) direction
κ_z = thermal conductivity in the depth (cross-plane) direction

References

[1] Chen, G., 2005, *Nanoscale Energy Transport and Conversion: A Parallel Treatment of Electrons, Molecules, Phonons, and Photons* (MIT-Pappalardo Series in Mechanical Engineering), Oxford University Press, New York.
[2] Brandrup, J., Immergut, E. H., Grulke, E. A., Abe, A., and Bloch, D. R., 1989, *Polymer Handbook*, Vol. 7, Wiley, New York.
[3] Sperling, L. H., 2005, *Introduction to Physical Polymer Science*, Wiley, New York.
[4] Shriver, J. W., 2009, *Protein Structure, Stability, and Interactions*, Springer, New York.
[5] Buchner, J., and Kiefhaber, T., 2005, *Protein Folding Handbook*, Vol. 3, Wiley-VCH, Weinheim, Germany.
[6] Braun, J. L., and Hopkins, P. E., 2017, "Upper Limit to the Thermal Penetration Depth During Modulated Heating of Multilayer Thin Films With Pulsed and Continuous Wave Lasers: A Numerical Study," J. Appl. Phys., **121**(17), p. 175107.
[7] Schmidt, A., Chiesa, M., Chen, X., and Chen, G., 2008, "An Optical Pump-Probe Technique for Measuring the Thermal Conductivity of Liquids," Rev. Sci. Instrum., **79**(6), p. 064902.
[8] Carslaw, H. S., and Jaeger, J. C., 1959, *Conduction of Heat in Solids*, 2nd ed., Clarendon Press, Oxford, UK.
[9] Capinski, W. S., Maris, H. J., Ruf, T., Cardona, M., Ploog, K., and Katzer, D. S., 1999, "Thermal-Conductivity Measurements of Gaas/Alas Superlattices Using a Picosecond Optical Pump-and-Probe Technique," Phys. Rev. B, **59**(12), pp. 8105–8113.
[10] Cahill, D. G., 2004, "Analysis of Heat Flow in Layered Structures for Time-Domain Thermoreflectance," Rev. Sci. Instrum., **75**(12), p. 5119.
[11] Schmidt, A. J., Chen, X., and Chen, G., 2008, "Pulse Accumulation, Radial Heat Conduction, and Anisotropic Thermal Conductivity in Pump-Probe Transient Thermoreflectance," Rev. Sci. Instrum., **79**(11), p. 114902.
[12] Bergman, T. L., Lavigne, A. S., Incropera, F. P., and DeWitt, D. P., 2011, *Fundamentals of Heat and Mass Transfer*, Wiley, Hoboken, NJ.
[13] Wang, X., Liman, C. D., Treat, N. D., Chabinyc, M. L., and Cahill, D. G., 2013, "Ultralow Thermal Conductivity of Fullerene Derivatives," Phys. Rev. B, **88**(7), p. 075310.
[14] George, M. C., Rodriguez, M. A., Kent, M. S., Brennecka, G. L., and Hopkins, P. E., 2015, "Thermal Conductivity of Self-Assembling Symmetric Block Copolymer Thin Films of Polystyrene-Block-Poly(Methyl Methacrylate)," ASME J. Heat Transfer, **138**(2), p. 024505.
[15] Guo, Z., Lee, D., Liu, Y., Sun, F., Sliwinski, A., Gao, H., Burns, P. C., Huang, L., and Luo, T., 2014, "Tuning the Thermal Conductivity of Solar Cell Polymers Through Side Chain Engineering," Phys. Chem. Chem. Phys., **16**(17), pp. 7764–7771.
[16] Touloukian, Y. S., Powell, R. W., Ho, C. Y., and Klemens, P. G., 1970, *Thermophysical Properties of Matter—Specific Heat: Non-Metallic Solids*, Vol. 5, IFI/Plenum, New York.
[17] Braun, J. L., Baker, C. H., Giri, A., Elahi, M., Artyushkova, K., Beechem, T. E., Norris, P. M., Leseman, Z. C., Gaskins, J. T., and Hopkins, P. E., 2016, "Size Effects on the Thermal Conductivity of Amorphous Silicon Thin Films," Phys. Rev. B, **93**, p. 140201(R).
[18] Haynes, W. M., 2014, *CRC Handbook of Chemistry and Physics*, CRC Press, Boca Raton, FL.
[19] Stevens, R. J., Smith, A. N., and Norris, P. M., 2005, "Measurement of Thermal Boundary Conductance of a Series of Metal-Dielectric Interfaces by the Transient Thermoreflectance Technique," ASME J. Heat Transfer, **127**(3), pp. 315–322.
[20] Hopkins, P. E., 2013, "Thermal Transport Across Solid Interfaces With Nanoscale Imperfections: Effects of Roughness, Disorder, Dislocations, and Bonding on Thermal Boundary Conductance," ISRN Mech. Eng., **2013**, p. 982586.
[21] Touloukian, Y. S., and Buyco, E. H., 1970, Thermophysical Properties of Matter—Specific Heat: Metallic Elements and Alloys, Vol. 4, IFI/Plenum, New York.
[22] Yang, J., Ziade, E., and Schmidt, A. J., 2016, "Modeling Optical Absorption for Thermoreflectance Measurements," J. Appl. Phys., **119**(9), p. 095107.
[23] Koh, Y. K., and Cahill, D. G., 2007, "Frequency Dependence of the Thermal Conductivity of Semiconductor Alloys," Phys. Rev. B, **76**, p. 075207.
[24] Regner, K. T., Sellan, D. P., Su, Z., Amon, C. H., McGaughey, A. J. H., and Malen, J. A., 2013, "Broadband Phonon Mean Free Path Contributions to Thermal Conductivity Measured Using Frequency Domain Thermoreflectance," Nat. Commun., **4**(3), p. 1640.
[25] Schmidt, A. J., 2013, "Pump-Probe Thermoreflectance," Annu. Rev. Heat Transfer, **16**, pp. 159–181.
[26] Hopkins, P. E., Serrano, J. R., Phinney, L. M., Kearney, S. P., Grasser, T. W., and Harris, C. T., 2010, "Criteria for Cross-Plane Dominated Thermal Transport in Multilayer Thin Film Systems During Modulated Laser Heating," ASME J. Heat Transfer, **132**(8), p. 081302.
[27] Costescu, R. M., Wall, M. A., and Cahill, D. G., 2003, "Thermal Conductance of Epitaxial Interfaces," Phys. Rev. B, **67**, p. 054302.
[28] Liu, J., Zhu, J., Tian, M., Gu, X., Schmidt, A., and Yang, R., 2013, "Simultaneous Measurement of Thermal Conductivity and Heat Capacity of Bulk and Thin Film Materials Using Frequency-Dependent Transient Thermoreflectance Method," Rev. Sci. Instrum., **84**(3), p. 034902.
[29] Oh, D.-W., Kim, S., Rogers, J. A., Cahill, D. G., and Sinha, S., 2011, "Interfacial Thermal Conductance of Transfer-Printed Metal Films," Adv. Mater., **23**(43), pp. 5028–5033.
[30] Duda, J. C., Yang, C. Y. P., Foley, B. M., Cheaito, R., Medlin, D. L., Jones, R. E., and Hopkins, P. E., 2013, "Influence of Interfacial Properties on Thermal Transport at Gold:Silicon Contacts," Appl. Phys. Lett., **102**(8), p. 081902.
[31] Cahill, D. G., 1990, "Thermal Conductivity Measurement From 30 to 750 K: The 3ω Method," Rev. Sci. Instrum., **61**(2), pp. 802–808.
[32] McPeak, K. M., Jayanti, S. V., Kress, S. J. P., Meyer, S., Iotti, S., Rossinelli, A., and Norris, D. J., 2015, "Plasmonic Films Can Easily Be Better: Rules and Recipes," ACS Photonics, **2**(3), pp. 326–333.
[33] Ge, Z., Cahill, D. G., and Braun, P. V., 2006, "Thermal Conductance of Hydrophilic and Hydrophobic Interfaces," Phys. Rev. Lett., **96**(18), p. 186101.
[34] Harikrishna, H., Ducker, W. A., and Huxtable, S. T., 2013, "The Influence of Interface Bonding on Thermal Transport Through Solid–Liquid Interfaces," Appl. Phys. Lett., **102**(25), p. 251606.
[35] Tian, Z., Marconnet, A., and Chen, G., 2015, "Enhancing Solid-Liquid Interface Thermal Transport Using Self-Assembled Monolayers," Appl. Phys. Lett., **106**(21), p. 211602.
[36] Hopkins, P. E., Kaehr, B., Phinney, L. M., Koehler, T. P., Grillet, A. M., Dunphy, D., Garcia, F., and Brinker, C. J., 2011, "Measuring the Thermal Conductivity of Porous, Transparent SiO_2 Films With Time Domain Thermoreflectance," ASME J. Heat Transfer, **133**(6), p. 061601.
[37] Hopkins, P. E., Kaehr, B., Piekos, E. S., Dunphy, D., and Jeffrey Brinker, C., 2012, "Minimum Thermal Conductivity Considerations in Aerogel Thin Films," J. Appl. Phys., **111**(11), p. 113532.
[38] Wang, L., Cheaito, R., Braun, J. L., Giri, A., and Hopkins, P. E., 2016, "Thermal Conductivity Measurements of Non-Metals Via Combined Time- and Frequency-Domain Thermoreflectance Without a Metal Film Transducer," Rev. Sci. Instrum., **87**(9), p. 094902.
[39] Wilson, R. B., and Cahill, D. G., 2014, "Anisotropic Failure of Fourier Theory in Time-Domain Thermoreflectance Experiments," Nat. Commun., **5**(10), p. 5075.
[40] Wilson, R. B., and Cahill, D. G., 2015, "Limits to Fourier Theory in High Thermal Conductivity Single Crystals," Appl. Phys. Lett., **107**(20), p. 203112.

Downloaded From: http://heattransfer.asmedigitalcollection.asme.org/ on 05/18/2018 Terms of Use: http://www.asme.org/about-asme/terms-of-use